NANO LETTERS

2007
Vol. 7, No. 5
1376−1380

Long-Range Surface Plasmons on Ultrathin Membranes

Pierre Berini,*,†,‡ Robert Charbonneau,† and Nancy Lahoud†

Spectalis Corp., 610 Bronson Avenue, Ottawa, Ontario K1S 4E6, Canada, and School of Information Technology and Engineering, University of Ottawa, 161 Louis Pasteur Street, Ottawa, Ontario K1N 6N5, Canada

Received February 26, 2007; Revised Manuscript Received March 30, 2007

ABSTRACT

A waveguide structure supporting long-range surface plasmon waves in any gaseous or liquid environment is described. The waveguide comprises a large area dielectric membrane of nanometric thickness upon which thin metal stripes and features are deposited. This structure allows the environment to surround the stripe thus ensuring that an essentially symmetric dielectric background is always present, as required to support the wave. The membrane perturbs the wave in a manner that significantly increases its surface sensitivity. The high surface sensitivity in concert with the ability to create long optical interaction length plasmonic structures leads to high sensitivity (bio)chemical sensors. Theoretical results describing the operation of the structure are given along with experimental results demonstrating the propagation of long-range surface plasmons in air and in liquid. The structure opens up a wealth of opportunities for research and application across many fields, including plasmonics, photonics, material science, surfaces, and solid–liquid interfaces.

Surface plasmon polaritons (SPPs)[1] are TM-polarized optical surface waves propagating along a metal−dielectric interface. They are known to be highly surface sensitive but also to have a high attenuation which can be a limiting factor for applications. Indeed, following decades of SPP research,[2,3] the most successful application remains (bio)chemical sensors to monitor bindings in real time between a molecule in solution and its complement immobilized along the surface of the metal film,[4−6] in the ever popular Kretschmann−Raether attenuated total reflection prism configuration.[1] Reducing the attenuation of SPPs and providing full confinement in the transverse plane while allowing propagation through any transparent gaseous or liquid medium would significantly open up the scope for basic and applied research with SPPs as well as offer new opportunities for application. The description of an SPP waveguide structure satisfying these requirements is the subject of this paper.

A practical way of reducing the SPP attenuation is to use a thin metal film bounded on both sides by the same dielectric and operating the structure in its symmetric SPP mode,[7−9] also termed the long-range SPP (LRSPP). Such a structure is shown in Figure 1a for $w = \infty$ and $\epsilon_1 = \epsilon_2$. This idea was taken one step further by limiting the width of the metal film, as shown in Figure 1a, thus defining a stripe along which an LRSPP mode can also propagate,[10−12] termed the long-range ss_b^0 mode in the nomenclature of ref 10. In this case, confinement is provided in the plane transverse to the direction of propagation, thus enabling plasmonic components such as bends, splitters, couplers, Mach−Zehnder interferometers,[13−15] and Bragg gratings[16,17] to be created in an integrated fashion. Metal stripes in strongly asymmetric environments ($\epsilon_1 < \epsilon_2$) have also been studied,[18−21] but the attenuation in these structures is generally high, near that of the single interface SPP.[1]

A requirement at the root of many problems and limiting the application of LRSPPs remains in that the structure (Figure 1a) must be symmetric ($\epsilon_1 = \epsilon_2$) to within a very tight tolerance in order for the LRSPP to be supported as a purely bound (nonradiative) mode. This symmetry requirement renders it rather difficult for LRSPPs to propagate in gaseous environments for instance since substrate materials that are index-matched to gases ($n_2 = n_1 \sim 1$) are not readily available. This requirement also poses serious problems for propagating LRSPPs in liquids. Not all liquids have an index-matched solid counterpart that could be used for the substrate, and even in cases where such a counterpart can be found, the tolerance required on the index matching imposes constraints on the liquid composition and temperature that may be limiting or impractical. Finally, a constraint to using well-understood and readily deposited materials might be desirable, ruling out nonmainstream materials.

We removed the limitations and constraints engendered by the symmetry requirement by eliminating the substrate altogether, replacing it with an ultrathin dielectric membrane

* Corresponding author: berini@site.uottawa.ca, pierreberini@spectalis.com.
† Spectalis Corp.
‡ University of Ottawa.

10.1021/nl070464w CCC: $37.00
Published on Web 04/13/2007

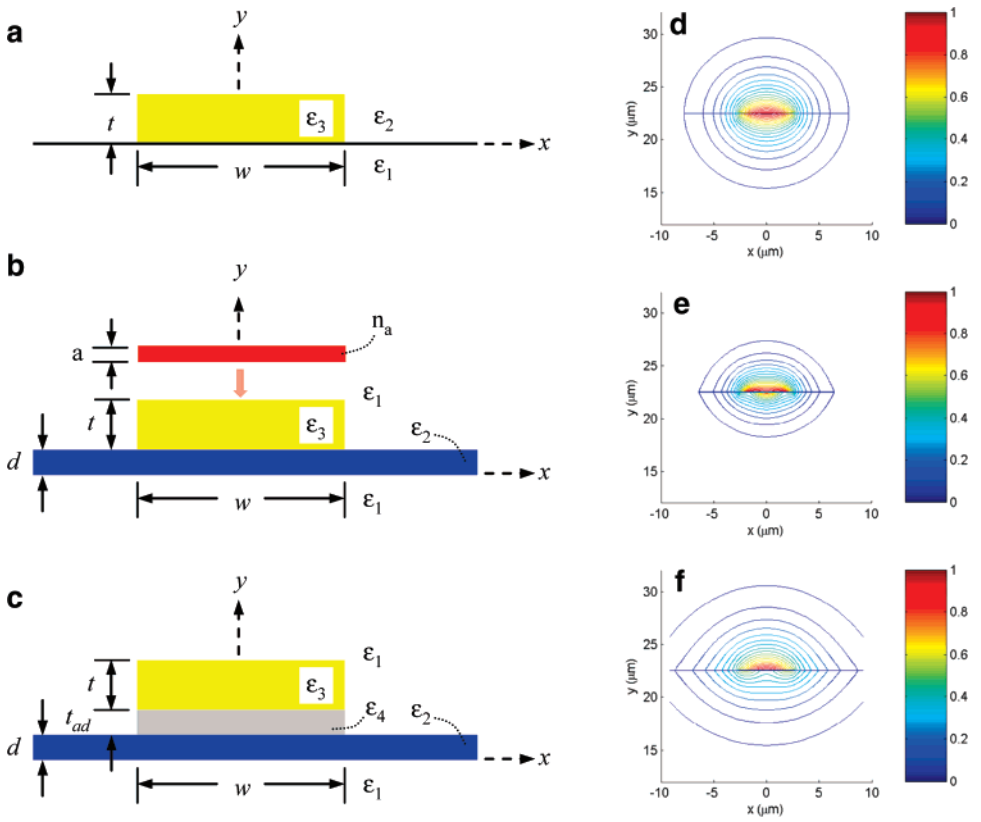

Figure 1. (a) Thin metal stripe of width w, thickness t, and permittivity ϵ_3 on a substrate of permittivity ϵ_1 and covered by a material of permittivity ϵ_2. (b) Metal stripe on a membrane of thickness d and permittivity ϵ_2 in an environment of permittivity ϵ_1. An idealized protein adlayer of thickness a and refractive index n_a is placed on top of the metal stripe to compute the surface sensitivity. (c) Introduction of an adhesion layer of thickness t_{ad} and permittivity ϵ_4. (d−f) Computed contours of Re$\{E_y\}$ of the LRSPP (ss_b^0 mode) supported by the structure in part b for $w = 5$ μm, $t = 25$ nm, and $\lambda_0 = 1310$ nm. Au and Si_3N_4 were selected as the materials of the stripe and membrane, respectively, and the fields are normalized such that max|Re$\{E_y\}$| = 1: (d) water is the environment and $d = 1$ nm; (e) water is the environment and $d = 20$ nm; (f) vacuum is the environment and $d = 20$ nm.

as the support for the metal stripe, and allowing the gaseous or liquid environment to surround the structure, as shown in Figure 1b. The modes supported by this "membrane waveguide" were generated numerically for different constructions. It was discovered that the LRSPP (the low-loss ss_b^0 mode (ref 10)) can be guided using practical membranes in gaseous and aqueous environments and that the LRSPP was perturbed by the membrane in a manner that favors surface sensing along the top metal surface. It was also determined that as long as the membrane remains optically thin enough the perturbation is not too strong and the LRSPP remains long-range.

The modes were obtained numerically by solving the vector wave equation subject to the applicable boundary conditions via the method of lines (MoL) as described in ref 10. The MoL is a highly accurate vectorial numerical technique and was validated experimentally for LRSPPs.[22] Au and Si_3N_4 were assumed as the materials for the stripe and membrane, respectively, with $w = 5$ μm and $t = 25$ nm, and the free-space wavelength of operation was set to $\lambda_0 = 1310$ nm. Parts d−f of Figure 1 show computed contours of the LRSPP for membranes of different thickness in water and vacuum. Figure 1d corresponds to the nominal situation where the membrane is essentially absent, having a thickness of $d = 1$ nm, and for water as the environment. Figure 1e corresponds to the situation of Figure 1d but for a membrane of thickness $d = 20$ nm. Figure 1f corresponds to the situation of Figure 1e but with vacuum as the environment instead of water.

The LRSPP is purely bound if its effective index (n_{eff}) is larger than that of the TM_0 mode supported by the membrane alone and larger than n_1. If these conditions are not met, then radiation leakage into the TM_0 mode of the membrane on either side of the metal stripe and into unbound waves supported by the background, respectively, can occur. Both conditions were indeed verified for the cases of parts d−f of Figure 1. Strictly speaking, the effective index of the LRSPP should also be larger than that of the TE_0 mode supported by the membrane alone, but these modes are substantially orthogonal. So as long as features in the waveguide or integrated structure do not cause LRSPP-TE_0 mode conversion, then leakage should not be observed irrespective of the relative magnitude of their effective indices. This was indeed verified experimentally, as described further below, for the case of Figure 1f (in air) where the effective index of the LRSPP is smaller than that of the TE_0 mode of the membrane alone.

Comparing parts d and e of Figure 1 reveals that the introduction of a thin membrane causes increased confinement and localization of the LRSPP to the top metal surface.

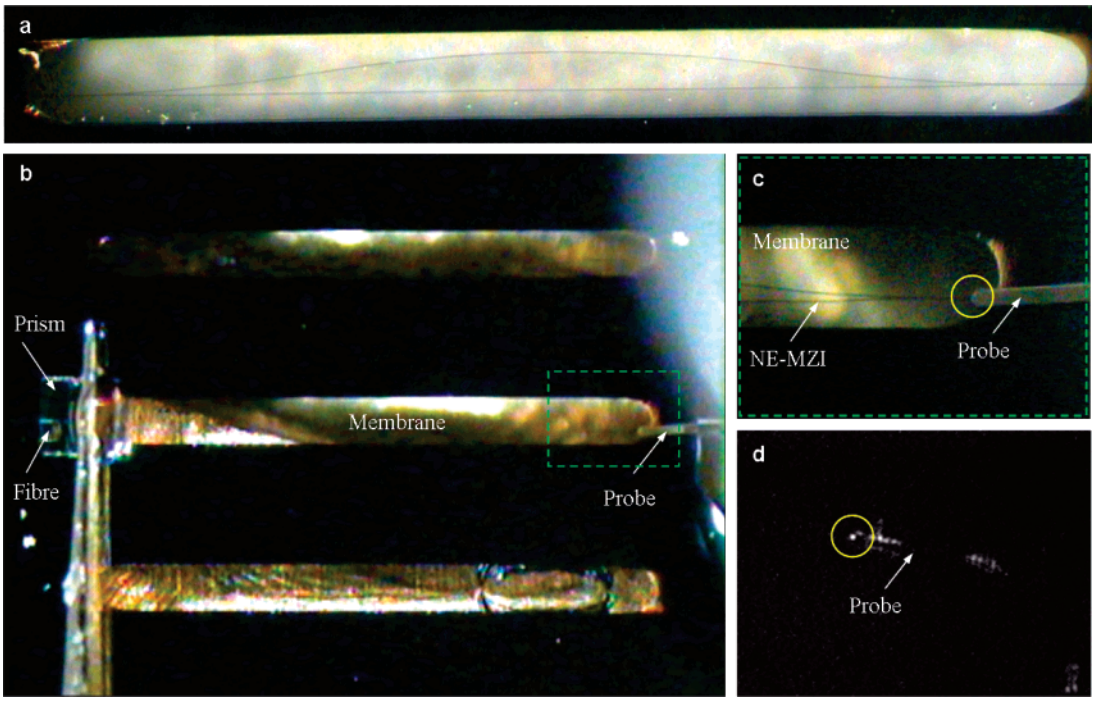

Figure 2. Mach−Zehnder interferometers (MZIs) on membranes. (a) Stitched microscope image of a full nonequal arm MZI (NE-MZI). The membrane width and length are about 340 μm and 3 mm, respectively. (b) Microscope image of the experimental setup showing three membrane structures immersed in optical fluid having an index close to that of water, each membrane bearing an MZI. The brass immersion bath is visible through the membranes, but the metal MZIs on the membranes are not apparent at this magnification. (c) High-magnification image of the region enclosed by the dashed green box in part b revealing the metal Y-junction combiner at the output of an NE-MZI and showing the AFM probe contacting the stripe. (d) Microscope image captured via infrared camera showing scattered light at $\lambda_0 = 1310$ nm originating from the LRSPP (ss_b^0 mode) propagating along the structure and caused by contacting the stripe with the probe as shown in part c. The bright spot at the center of the yellow circle corresponds to the contact point of the probe with the stripe.

These changes are accompanied by an increase in attenuation, but the attenuation, localization, and confinement are continuously variable with membrane thickness and index and, hence, are eminently adjustable. Comparing parts e and f of Figure 1 reveals that the same structure in vacuum has a more localized LRSPP but lower confinement. It is apparent from these contours that the membrane is more invasive in vacuum than in water, which is not surprising since the index contrast between the membrane material and the environment is greater in the case of vacuum.

From parts d and e of Figure 1, it is evident that the perturbation to the LRSPP caused by the membrane is useful to sensing applications where changes in an adlayer located along the top surface of the metal stripe are monitored. In order to illustrate this point, an idealized protein adlayer (thickness $a = 3$ nm and index $n_a = 1.5$) was placed on top of the stripe as suggested in Figure 1b and the surface sensitivity of the LRSPP defined as $\partial n_{eff}/\partial a$[23] was computed. Values of $\partial n_{eff}/\partial a = 0.55 \times 10^{-4}$ and 1.2×10^{-4} nm^{-1} were obtained for $d = 1$ and 20 nm (parts d and e of Figure 1), respectively, confirming that the perturbation is indeed beneficial. It is pointed out that the surface sensitivity, although high, is for a nonoptimised structure at $\lambda_0 = 1310$ nm.

It is also noted from parts d−f of Figure 1 that essentially 100% of the LRSPP fields are in the environment, which is a very useful feature for applications such as refractometric (bulk) sensing. The use of a liquid crystal or a gain medium in liquid or gaseous form as the environment also leads to interesting application possibilities.

We fabricated Au on Si_3N_4 membrane waveguides and components using a Si wafer as a support. Stoichiometric LPCVD Si_3N_4 was selected as the material for the membrane since tough high-quality tensile films are obtained. The material was deposited on Si wafers, and the membranes were released by applying Si etch processes from the backside. A contact aligner and bilayer photoresist were used in a liftoff process to define the metal features. Evaporation was used to coat the wafers, first with 2 nm of Cr as an adhesion layer, then with 23 nm of Au for a total metal stack thickness of 25 nm.

Figure 2a, the inset to Figure 3, and parts a and b of Figure 4 show microscope images of some fabricated structures. A typical metal stripe was characterized via atomic force microscopy (AFM) and found to be 5 μm wide and 25 nm thick, equal to the nominal values within experimental error. The root mean square surface roughness of the stripe was measured to be 0.77 nm. A typical Si_3N_4 membrane was characterized at many locations via ellipsometry and found to be on average 19.2 nm thick with a refractive index of 1.934 at $\lambda_0 = 1310$ nm. Assuming the covalent radii for Si and N, we estimate this membrane to be about 100 atoms thick. Many stripe bearing membranes of this thickness, and of various widths and lengths (typically hundreds of micrometers wide and millimeters long), were fabricated. The membranes are obviously fragile and must be handled with

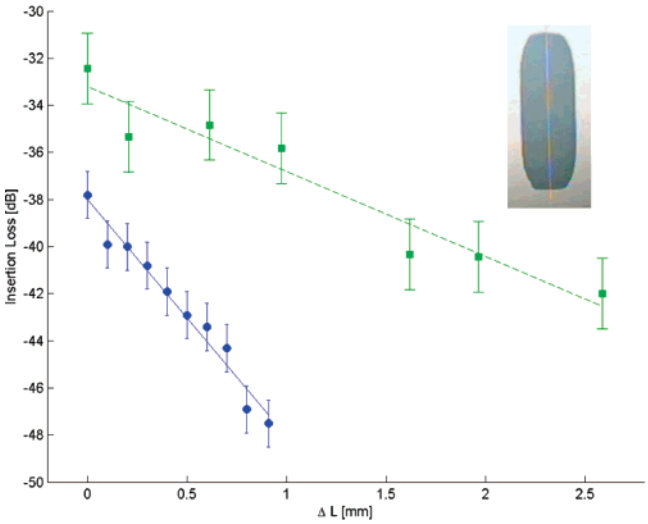

Figure 3. Measured insertion loss of the LRSPP (ss_b^0 mode) supported by membrane waveguides vs prism−probe separation ΔL. Air (■) and an optical fluid (●) with an index near that of water were selected as the environments. A typical membrane waveguide is shown as the microscope image in inset.

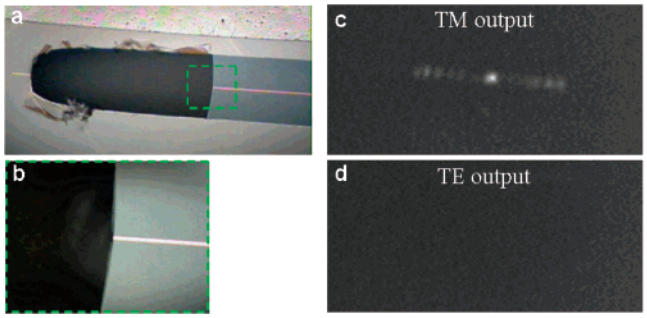

Figure 4. (a) Microscope image of a membrane waveguide obtained by cutting a full one with a focused ion beam and removing about half of the structure. (b) High-magnification image of the region enclosed by the dashed green box shown in part a. (c and d) Measured intensity distribution of the LRSPP (ss_b^0 mode) output from the waveguide at $\lambda_0 = 1310$ nm as viewed with an infrared camera and through an analyzer aligned parallel to, and normal to, the output transverse electric field, respectively. The waveguide is similar to that in Figure 3, and the environment is air.

care. Nonetheless, wafers bearing such membranes could be shipped using conventional wafer packaging, cleaned using typical aqueous solutions and solvents, and cleaved by scribing and breaking.

A custom experimental setup and procedures were devised to test the structures optically. The setup comprises an optical polarization maintaining fiber feeding an input prism coupler and a tipless AFM cantilever used as an output scattering probe. The structures are excited via evanescent proximity coupling along the top surface of the stripe using the prism. The output is obtained by contacting the stripe with the AFM cantilever and collecting a portion of the scattered light using an optical fiber or an infrared camera. The AFM cantilever was made to deflect (bend) slightly when contacting the membrane by applying a downward force.

Figure 2b shows a microscope image of the experimental setup with three membrane structures immersed in a basin containing optical fluid having an index close to that of water. Figure 2c is a high-magnification microscope image of the output region of the device under test, which in this case is a nonequal arm Mach−Zehnder interferometer similar to that shown in Figure 2a, with the AFM probe in physical contact with the metal stripe on the membrane. Figure 2d shows a high-magnification microscope image captured with an infrared camera showing scattered light at $\lambda_0 = 1310$ nm, originating from the LRSPP (ss_b^0 mode) propagating along the structure. The bright spot at the center of the yellow circle corresponds to the contact point of the probe with the stripe, as shown in Figure 2c. Measurements such as these were used repeatedly to verify the operation of many devices.

Figure 3 shows the measured insertion loss at $\lambda_0 = 1310$ nm of the LRSPP propagating along a typical membrane waveguide in air and immersed in an optical liquid (Cargille 1.3250) having a refractive index close to that of water.[24] The measured attenuations are 3.6 and 10 dB/mm in the air and liquid environments, respectively, obtained as the slopes of the linear models fitted to the insertion loss data. The R^2 goodness of fit of these linear models is 0.93 and 0.97, respectively.

The theoretical attenuations were computed using the MoL for the structure of Figure 1c, which includes the adhesion layer. The thickness and relative permittivity of the membrane were set to the values measured via ellipsometry at $\lambda_0 = 1310$ nm ($d = 19.2$ nm, $\epsilon_{r,2} = 1.934^2$). Since the thickness of the metal stripe was measured to be the same as the nominal thickness ($t = 25$ nm), then the nominal thicknesses for the Cr and Au layers were assumed, $t_{ad} = 2$ and $t = 23$ nm, respectively, and their measured relative permittivity at $\lambda_0 = 1310$ nm were adopted: $\epsilon_{r,4} = -0.46 - j40.37$ and $\epsilon_{r,3} = -86.08 - j8.32$.[25] The relative permittivity of air was taken as $\epsilon_{r,1} = 1$, and that of the Cargille 1.3250 fluid as $\epsilon_{r,1} = 1.3211^2 - j(2.7673 \times 10^{-7})$ at $\lambda_0 = 1310$ nm,[24] which is adjusted for our measurement temperature of 22 °C. This fluid was selected since its refractive index is close to that of water and is accurately known.

The theoretical attenuations are 3.83 and 9.39 dB/mm in the air and liquid environments, respectively, yielding errors of 6% and −6.5% compared to the corresponding experimental attenuations. The theoretical attenuations of the single interface SPP along the corresponding air−Au and liquid−Au interfaces are 23.6 and 55.1 dB/mm, respectively, so this particular membrane waveguide supports LRSPPs that propagate 6.2 and 5.9 times further. The range could be extended further by using a thinner Au stripe (say, 20 nm) and a less optically invasive membrane fabricated using a lower index dielectric. Using a lower index dielectric would also allow the membrane to be slightly thicker, potentially increasing its strength.

A membrane waveguide was then cut in half using a focused ion beam and one of the portions removed, as shown in parts a and b of Figure 4, in order to insert a micromirror into the gap for viewing the output light with an infrared camera. Figure 4c shows the output captured for the waveguide in air, with an analyzer placed in front of the camera and aligned along the main transverse electric field

component of the output (E_y of the LRSPP). A TM output is observed, as expected, along with some radiation trapped in the membrane on either side, likely due to imperfect input coupling into the LRSPP. Rotating the analyzer by 90° produces the image shown in Figure 4d revealing an absence of TE light. Hence, no LRSPP-TE_0 mode conversion is observed.

A waveguide structure suitable for propagating LRSPPs in any gaseous or liquid environment was described. The structure comprises a large area ultrathin dielectric membrane upon which a thin metal stripe is deposited. The environment (gaseous or liquid) is allowed to surround the structure, effectively becoming the claddings. Si_3N_4 membranes ~0.3 × 3 mm^2 and ~100 atoms thick supporting 25 nm thick 5 μm wide Au stripes were fabricated, and the propagation of LRSPPs in air and liquid was demonstrated. The attenuation of the LRSPP in these media was measured, and the results compared very well with theory. The ability to propagate LRSPPs through any transparent gaseous or liquid medium opens up a wealth of basic and applied research paths. Advantageously, the same waveguide structure can be used regardless of the environment. Gain media, conveniently available in the gaseous or liquid states, can be used, and given the low loss of the LRSPP, net gain and lasing in this mode should be possible at many wavelengths. Experimental studies of fluorescence and spontaneous emission[26] from dipoles in solution into LRSPPs are also conveniently enabled. The high sensitivity of the LRSPP to the top metal surface, coupled with the low attenuation and the two-dimensional confinement provided in the transverse plane, enable integrated long-range plasmonic circuits[13−17] such as optically long Mach−Zehnder interferometers, leading to highly sensitive gas and (bio)chemical sensors. For bio-chemical sensors, using the Au stripe as the sensing surface is advantageous given the availability and maturity of stable self-assembled monolayers on this metal.[27]

References

(1) Raether, H. *Surface Plasmons on Smooth and Rough Surfaces and on Gratings*; Springer: Berlin, 1988.
(2) Barnes, W. L.; Dereux, A.; Ebbesen, T. W. *Nature* **2003**, *424*, 824.
(3) Maier, S. A.; Atwater, H. A. *J. Appl. Phys.* **2005**, *98*, 011101.
(4) Liedberg, B.; Nylander, C.; Lundstrom, I. *Sens. Actuators* **1983**, *4*, 299.
(5) Malmqvist, M. *Nature* 1993, *361*, 186.
(6) Homola, J.; Yee, S. S.; Gauglitz, G. *Sens. Actuators, B* **1999**, *54*, 3.
(7) Sarid, D. *Phys. Rev. Lett.* **1981**, *47*, 1927.
(8) Burke, J. J.; Stegeman, G. I.; Tamir, T. *Phys. Rev. B* **1986**, *33*, 5186.
(9) Yang, F.; Sambles, J. R.; Bradberry, G. W. *Phys. Rev. B* **1991**, *44*, 5855.
(10) Berini, P. *Phys. Rev. B* **2000**, *61*, 10484.
(11) Charbonneau, R.; Berini, P.; Berolo, E.; Lisicka-Shrzek, E. *Opt. Lett.* **2000**, *25*, 844.
(12) Nikolajsen, R.; Leosson, K.; Salakhutdinov, I.; Bozhevolnyi, S. I. *Appl. Phys. Lett.* **2003**, *82*, 668.
(13) Charbonneau, R.; Lahoud, N.; Mattiussi, G.; Berini, P. *Opt. Express* **2005**, *13*, 977.
(14) Boltasseva, A.; Nikolajsen, T.; Leosson, K.; Kjaer, K.; Larsen, M. S.; Bozhevolnyi, S. I. *J. Lightwave Technol.* **2005**, *23*, 413.
(15) Charbonneau, R.; Scales, C.; Breukelaar, I.; Fafard, S.; Lahoud, N.; Mattiussi, G.; Berini, P. *J. Lightwave Technol.* **2006**, *24*, 477.
(16) Jetté-Charbonneau, S.; Charbonneau, R.; Lahoud, N.; Mattiussi, G.; Berini, P. *Opt. Express* **2005**, *13*, 4674.
(17) Boltasseva, A.; Bozhevolnyi, S. I.; Søndergaard, T.; Nikolajsen, T.; Leosson, K. *Opt. Express* **2005**, *13*, 4237.
(18) Berini, P. *Phys. Rev. B* **2001**, *63*, 125417.
(19) Weeber, J.-C.; Dereux, A.; Girard, C.; Krenn, J. R.; Goudonnet, J.-P. *Phys. Rev. B* **1999**, *60*, 9061.
(20) Lamprecht, B.; Krenn, J. R.; Schider, G.; Ditlbacher, H.; Salerno, M.; Felidj, N.; Leitner, A.; Aussenegg, F. R. *Appl. Phys. Lett.* **2001**, *79*, 51.
(21) Weeber, J.-C.; Krenn, J. R.; Dereux, A.; Lamprecht, B.; Lacroute, Y.; Goudonnet, J.-P. *Phys. Rev. B* **2001**, *64*, 045411.
(22) Berini, P.; Charbonneau, R.; Lahoud, N.; Mattiussi, G. *J. Appl. Phys.* **2005**, *98*, 043109.
(23) Tiefenthaler, K.; Lukosz, W. *J. Opt. Soc. Am. B* **1989**, *6*, 209.
(24) Cargille Labs, www.cargille.com.
(25) *Handbook of Optical Constants of Solids*; Palik, E. D., Ed.; Academic Press: Orlando, FL, 1985.
(26) Barnes, W. L. *J. Mod. Opt.* **1998**, *45*, 661.
(27) Love, J. C.; Estroff, L. A.; Kriebel, J. K.; Nuzzo, R. G.; Whitesides, G. M. *Chem. Rev.* **2005**, *105*, 1103.

NL070464W